positive for CD11b and negative for CD90 (Fig. 3b, d). Only 0.047% of cultured cells were CD-90-positive and CD-45-negative, consistent with MSC characteristics (Fig. 3d). Flow cytometric analysis showed that mainly macrophage fractions were increased in the cultured system; these cells were subsequently used in our study.

Improvement in serum albumin after BMC and cultured BMC infusion

Serum albumin was lower in the CCl_4 injury group (group A) but was significantly higher in the BMC-treatment group (group B) and the cultured cell-treatment group (group C). No significant differences were apparent between groups B and C (Fig. 4). These results showed that the improvement of liver function was similar between primary BMC and 1/10 the amount of cultured BMC. Except for the serum albumin levels, no significant differences were observed in other blood data (e.g., alanine aminotransferase, total bilirubin; data not shown) between the three groups.

Improvement in liver fibrosis after BMC and cultured BMC infusion

Liver fibrosis was evaluated by Sirius-red staining. As compared with the CCl_4 injury group (group A), the fibrosis area was smaller in the BMC-treatment group and cultured-cell-treatment group (Fig. 5a-d). In groups B and C, GFP-positive cells were mainly observed in the portal region (Fig. 5e-h). In addition, MMP-9 expression was significantly elevated in groups B and C (Fig. 5i-l). Immunohistochemical analysis showed a few F4/80-positive cells around the liver in groups A and B (Fig. 6a, b). On the other hand, in group C, many F4/80-positive cells were mainly observed in the portal region (Fig. 6c). Double-immunostaining revealed that a few F4/80/

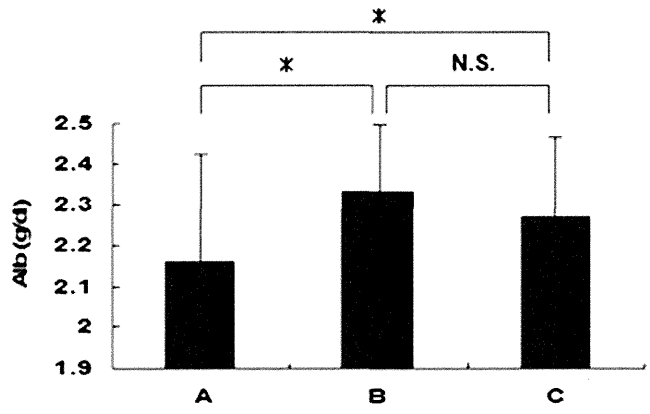

Fig. 4 Serum albumin (*Alb*). After 8 weeks of treatment with CCl_4 (4 weeks after BMC/cultured cell administration), mouse blood was collected and analyzed. CCl_4 group (*A*), CCl_4 + BMC group (*B*), and CCl_4 + cultured cell group (*C*). *$P<0.05$ (*N.S.* not significant)

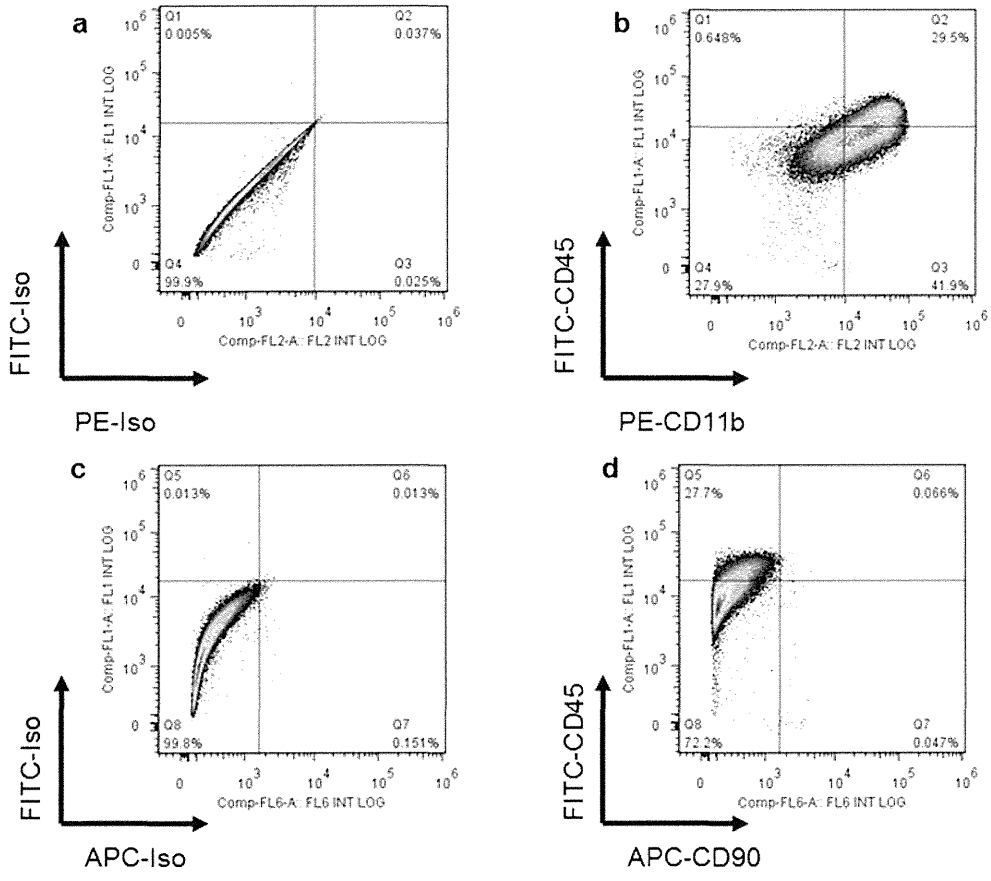

Fig. 3 Cellular characterization of cultured BMCs by flow cytometric analysis. Representative flow cytometric analyses for CD11b, CD45 and CD90 antigens in bone-marrow-derived cultured cells. **a** Isotype (*Iso*) control for phycoreythrin (*PE*)- and fluorescein isothiocyanate (*FITC*)-conjugated antibodies. **b** Expression of CD11b (*x-axis*) and CD45 (*y-axis*). **c** Isotype control for allophycocyanin (*APC*)- and fluorescein isothiocyanate (*FITC*)-conjugated antibodies. **d** Expression of CD90 (*x-axis*) and CD45 (*y-axis*)

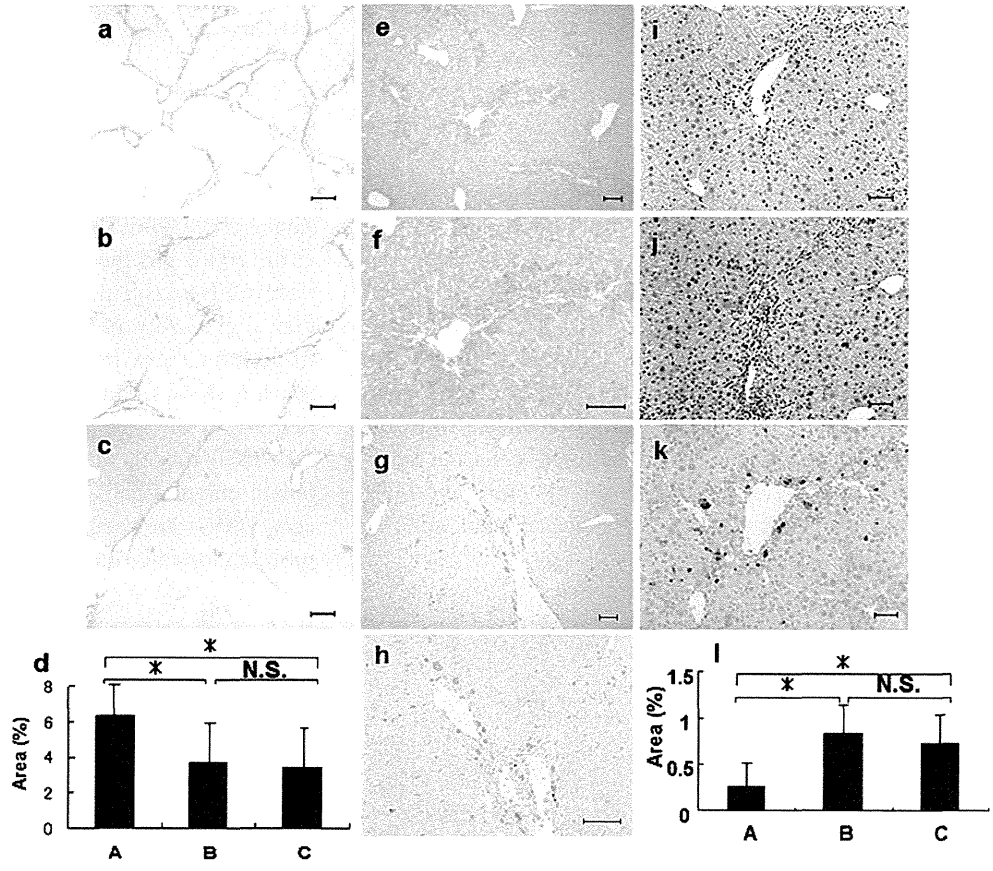

Fig. 5 Sirius-red staining; immunohistochemical analysis of GFP and metalloproteinase-9 (MMP-9) expression in liver. After 8 weeks of treatment with CCl_4 (4 weeks after BMC/cultured cell administration), livers from all mice were resected. **a-d** Sirius-red staining. **a** CCl_4 group. **b** CCl_4 + BMC group. **c** CCl_4 + cultured cell group. Magnification ×40. **d** Image analysis of the Sirius red-positive area. CCl_4 group (*A*), CCl_4 + BMC group (*B*), CCl_4 + cultured cell group (*C*). **P*<0.05 (*N.S.* not significant). **e–h** Immunostaining for GFP. **e** CCl_4 + BMC group. Magnification ×100. **f** Magnified view of **e**. Magnification ×200. **g** CCl_4 + cultured cell group. Magnification ×100. **h** Magnified view of **g**. Magnification ×200. **i–l** Immunostaining for MMP-9. **i** CCl_4 group. **j** CCl_4 + BMC group. **k** CCl_4 + cultured cell group. Magnification ×200. **l** Image analysis of the MMP-9-positive area (*A–C* as in **d**). **P*<0.05 (*N.S.* not significant). *Bars* 100 μm (**a–c**, **e-k**)

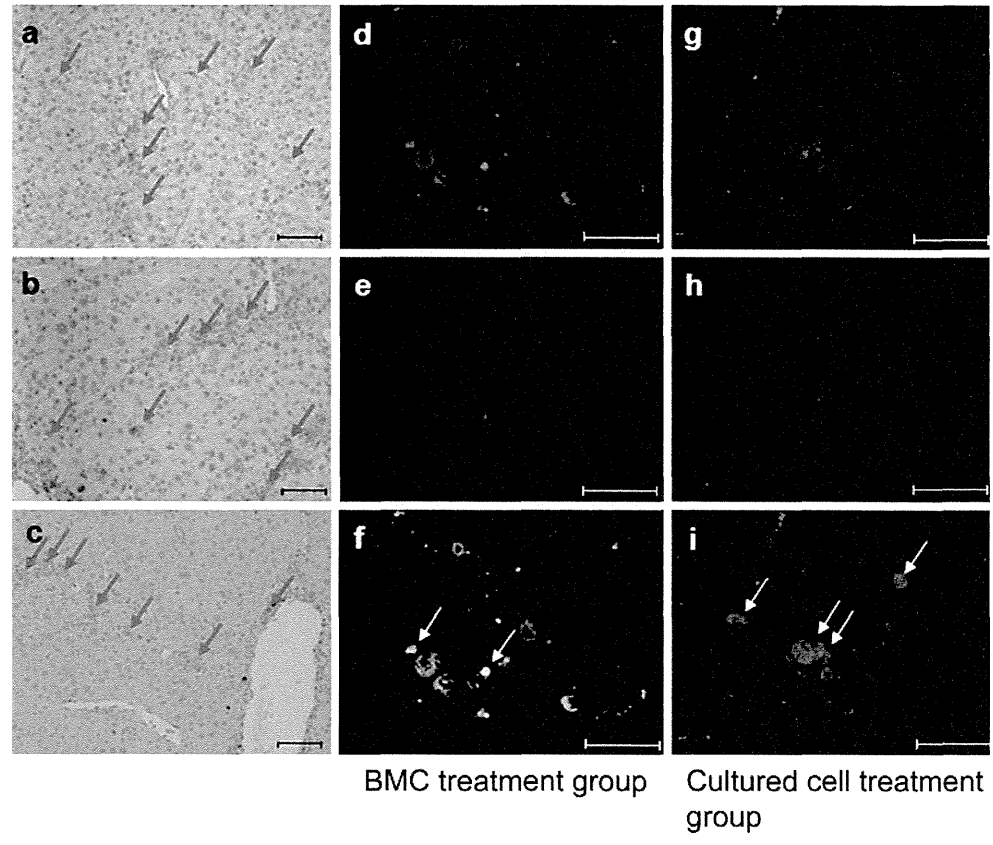

Fig. 6 Immunohistochemical analysis of F4/80 expression in liver. After 8 weeks of treatment with CCl_4 (4 weeks after BMC/cultured cell administration), the livers from all mice were resected. **a–c** Immunostaining for F4/80 (*red arrows* F4/80-positive cells). **a** CCl_4 group. **b** CCl_4 + BMC group. **c** CCl_4 + cultured cell group. Magnification ×100. **d–f** BMC-treatment group (*BMC treatment group*). **d** GFP (*green*). **e** F4/80 (*red*. **f** GFP (*green*), F4/80 (*red*), GFP and F4/80 (*yellow*). Note the GFP/F4/80 double-positive cells (*white arrows*). Magnification ×200. **g–i** Cultured-cell-treatment group (*Cultured cell treatment group*). **g** GFP (*green*), **h** F4/80 (*red*. **i** GFP and F4/80 (*yellow*). Note the GFP/F4/80 double-positive cells (*white arrows*). Magnification ×200. *Bars* 100 μm (**a–c**), 50 μm (**d–i**)

GFP double-positive cells were present in group B, whereas numerous F4/80/GFP-positive cells were observed in group C (Fig. 6d-i). These results showed that a higher number of F4/F80 cells had repopulated into the cirrhosis liver after cultured BMC infusion.

In order to characterize GFP-positive cells in the liver, we performed double-immunostaining. In the BMC-treatment group, numerous cells with co-positivity for GFP and MMP-9 were seen (Fig. 7a-c) but cells with co-positivity for GFP and α-SMA were not observed (Fig. 7d-f). In the cultured-cell-treatment group, the results were similar (Fig. 7g-l). These findings suggest that MMP-9 was mainly secreted from the migrating infused GFP-positive cultured cells. In addition, a few cells were co-positive for vimentin and GFP, thus indicating graft survival of mesenchymal cells in the liver (Fig. 7m-o).

Discussion

In this study, we cultured bone-marrow-derived cells by using serum-free medium and analyzed their ability to improve liver cirrhosis. Several studies of cultured bone-marrow-derived cells have been reported (Wu et al. 2005; Zheng et al. 2006; Fang et al. 2004; Zhao et al. 2005; Oyagi et al. 2006) but the culture of bone-marrow-derived cells from GFP-transgenic mice has been difficult, because of their decreased proliferation potential (Peister et al. 2004). In addition, in a previous study conducted with cultured murine BMCs, numerous macrophages were reported (Tropel et al. 2004). Employing a previously reported GFP/CCl_4 model, we first improved the culture methods to obtain cultured cells efficiently. In standard culture protocols, BMCs are seeded at a density of $1\times10^{5\sim6}$/ml but the proliferation rate is insufficient (Soleimani and Nadri 2009).

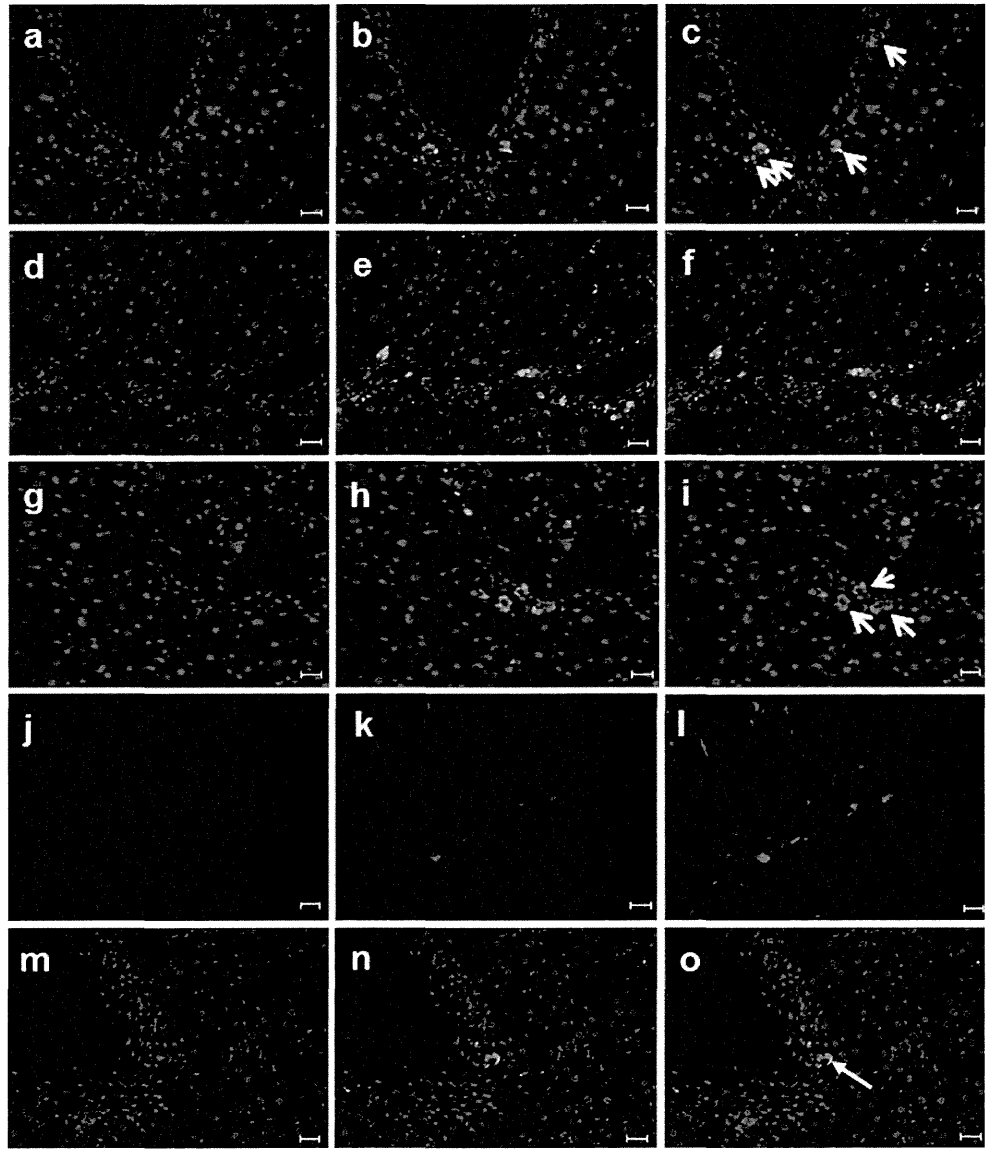

Fig. 7 Double-immunostaining (BMC group vs. cultured cell group). After 8 weeks of treatment with CCl_4 (4 weeks after BMC/cultured cell administration), the livers from all mice were resected. **a–f** BMC treatment group. **a** MMP-9 (*red*). **b** GFP (*green*). **c** MMP-9 (*red*)/GFP (*green*)/GFP and MMP-9 (*yellow*). Note the co-positive cells (*short white arrows*). **d** α-SMA (*red*). **e** GFP (*green*). **f** α-SMA (*red*)/GFP (*green*). Magnification ×100. **g–o** Cultured-cell-treatment group. **g** MMP-9 (*red*). **h** GFP (*green*). **i** MMP-9 (*red*)/GFP (*green*)/GFP and MMP-9 (*yellow*). Note the co-positive cells (*short white arrows*). **j** α-SMA (*red*). **k** GFP (*green*). **l** α-SMA (*red*)/GFP (*green*)/α-SMA and GFP (*yellow*). **m** Vimentin (*red*). **n** GFP (*green*). **o** Vimentin (*red*)/GFP (*green*)/vimentin and GFP (*yellow*). Note the co-positive cells (*long white arrow*). Magnification ×100. *Bars* 50 μm (**a–o**)

By increasing the cell density for primary culture to 1×10^7/ml, we found that BMCs could be grown more efficiently. Serum and fibroblast growth factor are usually added to the medium (Zheng et al. 2006) but bcause of the possibility of clinical application, we used serum-free medium and GMP-grade reagents (Agata et al. 2009). As shown in Fig. 2, by 2 weeks after cultivation, a sufficient number of cells was obtained. Moreover, the administered fraction had a high percentage of cells positive for CD11b and CD45 (Fig. 3).

Our macrophage fractions taken from mouse bone marrow increased by simply seeding them onto plastic in the presence of serum-free medium and GMP-grade reagents. With the administration of GFP-transgenic mice bone-marrow-derived cultured cells, we confirmed GFP-positive cells in the liver and like the GFP/CCl_4 model that we had previously reported, serum albumin increased and fibrosis improved in the treated mice (Figs. 4, 5a-d). Moreover, for this improvement effect, the number of administered cells was 1×10^4 cells/body, i.e., only 1/10 the usual amount, whereas the effects, as compared with conventional bone marrow administration, were not inferior.

In addition, double-immunostaining was performed to characterize the GFP-positive cells in the liver. Similarly, as we have earlier reported, there was co-expression of MMP-9 but cells co-expressing α-SMA were not observed (Fig. 6a-l; Sakaida et al. 2004; Higashiyama et al. 2007). The presence of GFP-positive cells co-expressing F4/80 was confirmed (Fig. 6) and, whereas GFP-positive cells co-expressing vimentin were also found, their number was low (Fig. 7m-o; Fang et al. 2004). These findings suggest that numerous cultured macrophages and some MSCs had repopulated the liver. As shown in Fig. 3, we infused mainly a macrophage fraction from our culturing system. Hence, we consider it reasonable that more F4./80/GFP-positive cells were found in the cultured BMC group than the primary BMC culture groups. In this mice study, we believe that the macrophage fraction mainly improved liver fibrosis. However, we need to examine which of the fractions are more effective for liver regeneration therapy.

We used a StemPro MSC Xeno Free medium to expand the mouse BMCs. Under these conditions, many macrophages were obtained and these macrophages contributed to the observed liver regeneration. On the other hand, in humans, MSCs are expanded under similar conditions. The reason for this might be attributable to species differences. Further studies will be required to understand the mechanism of this difference.

In the present study, bone-marrow-derived cells cultured with a serum-free medium clearly had an effect on repairing liver fibrosis. These results are important for translational research on cultured bone-marrow-derived cell therapy for liver cirrhosis. Issues for further investigation include an examination of the most effective cell fraction for improving liver fibrosis and whether the present system can reliably yield cultured cells from human BMCs. Studies analyzing the possibility of using human BMCs for cell therapy in liver cirrhosis are urgently needed.

Acknowledgments We are grateful to Ms. Mariko Yamada, Ms. Ihoko Fujimoto and Ms. Yoko Fukuzumi for assistance with cell culture, immunohistochemical analysis and animal care.

References

Agata H, Watanabe N, Ishii Y, Kubo N, Ohshima S, Yamazaki M, Tojo A, Kagami H (2009) Feasibility and efficacy of bone tissue engineering using human bone marrow stromal cells cultivated in serum-free conditions. Biochem Biophys Res Commun 382:353–358

Fang LJ, Fu XB, Cheng B, Sun TZ, Li JF, Cao R, Wang YX (2004) Study on the potentiation of bone marrow mesenchymal stem cells involved in sebaceous duct formation. Zhonghua Wai Ke Za Zhi 42:1136–1138

Friedenstein AJ, Latzinik NW, Grosheva AG, Gorskaya UF (1982) Marrow microenvironment transfer by heterotopic transplantation of freshly isolated and cultured cells in porous sponges. Exp Hematol 10:217–227

Higashiyama R, Inagaki Y, Hong YY, Kushida M, Nakao S, Niioka M, Watanabe T, Okano H, Matsuzaki Y, Shiota G, Okazaki I (2007) Bone marrow-derived cells express matrix metalloproteinases and contribute to regression of liver fibrosis in mice. Hepatology 45:213–222

Jin H, Yamamoto N, Uchida K, Terai S, Sakaida I (2007) Telmisartan prevents hepatic fibrosis and enzyme-altered lesions in liver cirrhosis rat induced by a choline-deficient L-amino acid-defined diet. Biochem Biophys Res Commun 364:801–807

Kim JK, Park YN, Kim JS, Park MS, Paik YH, Seok JY et al (2010) Autologous bone marrow infusion activates the progenitor cell compartment in patients with advanced liver cirrhosis. Cell Transplant 19:1237–1246

Oyagi S, Hirose M, Kojima M, Okuyama M, Kawase M, Nakamura T, Ohgushi H, Yagi K (2006) Therapeutic effect of transplanting HGF-treated bone marrow mesenchymal cells into CCl_4-injured rats. J Hepatol 44:742–748

Peister A, Mellad JA, Larson BL, Hall BM, Gibson LF, Prockop DJ (2004) Adult stem cells from bone marrow (MSCs) isolated from different strains of inbred mice vary in surface epitopes, rates of proliferation, and differentiation potential. Blood 103:1662–1668

Pittenger MF, Mackay AM, Beck SC, Jaiswal RK, Douglas R, Mosca JD, Moorman MA, Simonetti DW, Craig S, Marshak DR (1999) Multilineage potential of adult human mesenchymal stem cells. Science 284:143–147

Saito T, Okumoto K, Haga H, Nishise Y, Ishii R, Sato C, Watanabe H, Okada A, Ikeda M, Togashi H, Ishikawa T, Terai S, Sakaida I, Kawata S (2011) Potential therapeutic application of intravenous autologous bone marrow infusion in patients with alcoholic liver cirrhosis. Stem Cells Dev 20:1503–1510

Sakaida I, Terai S, Yamamoto N, Aoyama K, Ishikawa T, Nishina H, Okita K (2004) Transplantation of bone marrow cells reduces CCl_4-induced liver fibrosis in mice. Hepatology 40:1304–1311

Soleimani M, Nadri S (2009) A protocol for isolation and culture of mesenchymal stem cells from mouse bone marrow. Nat Protoc 4:102–106

Terai S, Sakaida I (2011) Autologous bone marrow cell infusion therapy for liver cirrhosis patients. J Hepatobiliary Pancreat Sci 18:23–25

Terai S, Sakaida I, Yamamoto N, Omori K, Watanabe T, Ohata S, Katada T, Miyamoto K, Shinoda K, Nishina H, Okita K (2003) An in vivo model for monitoring trans-differentiation of bone marrow cells into functional hepatocytes. J Biochem (Tokyo) 134:551–558

Terai S, Sakaida I, Nishina H, Okita K (2005) Lesson from the GFP/CCl_4 model—translational research project: the development of cell therapy using autologous bone marrow cells in patients with liver cirrhosis. J Hepatobiliary Pancreat Surg 12:203–207

Terai S, Ishikawa T, Omori K, Aoyama K, Marumoto Y, Urata Y, Yokoyama Y, Uchida K, Yamasaki T, Fujii Y, Okita K, Sakaida I (2006) Improved liver function in patients with liver cirrhosis after autologous bone marrow cell infusion therapy. Stem Cells 24:2292–2298

Thomas JA, Pope C, Wojtacha D, Robson AJ, Gordon-Walker TT, Hartland S, Ramachandran P, Van Deemter M, Hume DA, Iredale JP, Forbes SJ (2011) Macrophage therapy for murine liver fibrosis recruits host effector cells improving fibrosis, regeneration, and function. Hepatology 53:2003–2015

Tropel P, Noël D, Platet N, Legrand P, Benabid AL, Berger F (2004) Isolation and characterisation of mesenchymal stem cells from adult mouse bone marrow. Exp Cell Res 295:395–406

Wu LM, Li LD, Liu H, Ning KY, Li YK (2005) Effects of Guiyuanfang and autologous transplantation of bone marrow stem cells on rats with liver fibrosis. World J Gastroenterol 11:1155–1160

Zhao DC, Lei JX, Chen R, Yu WH, Zhang XM, Li SN, Xiang P (2005) Bone marrow-derived mesenchymal stem cells protect against experimental liver fibrosis in rats. World J Gastroenterol 11:3431–3440

Zheng JF, Liang LJ, Wu CX, Chen JS, Zhang ZS (2006) Transplantation of fetal liver epithelial progenitor cells ameliorates experimental liver fibrosis in mice. World J Gastroenterol 12:7292–7298

Biochemical and Biophysical Research Communications 422 (2012) 22–27

Contents lists available at SciVerse ScienceDirect

Biochemical and Biophysical Research Communications

journal homepage: www.elsevier.com/locate/ybbrc

Ezetimibe reduces fatty acid quantity in liver and decreased inflammatory cell infiltration and improved NASH in medaka model

Toshiyuki Oishi [a], Shuji Terai [a,*], Shinya Kuwashiro [a], Koichi Fujisawa [a], Toshihiko Matsumoto [a], Hiroshi Nishina [b], Isao Sakaida [a]

[a] Department of Gastroenterology & Hepatology, Yamaguchi University, Graduated School of Medicine, Minami Kogushi 1-1-1, Ube, Yamaguchi 755-8505, Japan
[b] Department of Developmental and Regenerative Biology, Medical Research Institute, Tokyo Medical and Dental University, 1-5-45, Yushima, Bunkyo-ku, Tokyo 113-8510, Japan

ARTICLE INFO

Article history:
Received 17 April 2012
Available online 25 April 2012

Keywords:
NASH
Ezetimibe
Medaka
Inflammation

ABSTRACT

Purpose: We previously developed medaka non-alcoholic steatohepatitis (NASH) model. The model showed similar histology with human NASH so we analyzed the effect of drug using medaka NASH activity score (MNAS). In this study we analyzed the effect of ezetimibe, a small intestine cholesterol transporter inhibitor, on NASH.
Methods: Medaka NASH model showed steatohepatits with infiltration of D-PAS positive inflammatory cell. In this study we induced medaka NASH and compared the effect of ezetimibe on medaka NASH by HFD.
Results: As compared with the HFD group, ezetimibe reduced total cholesterol and triacyglycerol in the blood. But concerning with liver quantity of fatty acids in the liver were significantly decreased by ezetimibe. Genes related with fatty acid metabolism in liver was also decreased by ezetimibe administration. On histological observations of the liver, increases in the number of inflammatory cells and MNAS were inhibited. With this decrease of fatty acid in liver, medaka NASH was improved by ezetimibe.
Conclusion: Ezetimibe was clarified as a useful drug to improve NASH.

1. Introduction

Non-alcoholic steatohepatitis (NASH) is a disease concept first reported by Ludwig et al. in 1980 [1]. The disease state resembles alcoholic liver disease, even though alcohol consumption is not noted in amounts sufficient to cause liver damage. It progresses from simple fatty liver to steatohepatitis and cirrhosis, and finally to hepatocarcinogenesis [1]. The number of patients with NASH is currently increasing worldwide, with the most widely supported theory on the cause of NASH being the two-hit theory proposed by Day et al., in which fatty liver occurs first (first hit), followed by a transition to steatohepatitis (second hit) [2]. However, the specific onset mechanisms of NASH have not yet been adequately elucidated. The thinking to date is that the first hit of fatty liver occurs against a background of symptoms including hypertension, dyslipidemia and glucose intolerance, comprising so-called metabolic syndrome, which then progresses to NASH as a result of unknown factors [2]. NASH further progresses to cirrhosis, and finally to hepatocarcinogenesis.

There are currently no established effective treatments for NASH, and the mechanism of the progression from simple fatty liver to NASH has not been completely elucidated either. Mice, rats and other rodents have been widely used in basic studies on NASH, but small fish, such as zebrafish, have also come to be recognized as useful model animals.

Medaka are small fish similar to zebrafish that are native to many parts of Japan and Asia. In Japan, there are numerous pure line species used as animal models [3]. Furthermore, in comparison with rodents, medaka reproduce prolifically, mature rapidly and are small; thus, little space and cost are required for breeding. The medaka genome project has also been completed, and methods have been established for the generation of transgenic and knockout animals, thereby fulfilling the necessary conditions for animal models [4]. Past reports on models with liver fatty changes in small fish include zebrafish mutants (*foie gras* mutants) [5], mutant medaka identified via genetic screening by *N*-ethyl-*N*-nitrosourea (ENU) treatment (Kendama mutants) [6], and a zebrafish model with liver fat accumulation due to expression of HBx protein [7]. In these reports, however, the models were prepared using mutants or genetic manipulation, and as of this writing, the only model exhibiting a profile resembling human NASH through feeding wild-type medaka a high-fat diet is our previously reported medaka NASH model [8].

After developing this human-like medaka NASH model [8], we demonstrated that it presents a pathological condition similar to human NASH, and that n-3 polyunsaturated fatty acid is very important in NASH pathology [8]. We have also demonstrated that

* Corresponding author. Fax: +81 836 22 2303.
E-mail address: terais@yamaguchi-u.ac.jp (S. Terai).

0006-291X/$ - see front matter © 2012 Elsevier Inc. All rights reserved.
http://dx.doi.org/10.1016/j.bbrc.2012.04.087

telmisartan, which has angiotensin II type 1 receptor-inhibiting and PPAR-γ-stimulating actions, inhibits liver macrophage infiltration and inhibits the accumulation of liver fat, thereby improving the pathological condition of the medaka NASH model [9]. In the present study, we administered ezetimibe, a small intestine cholesterol transporter (Niemann–Pick C1-Like 1) inhibitor, to the medaka NASH model, and clarified the effects of ezetimibe in this model.

2. Materials and methods

2.1. Animals

Himedaka strain Cab (an orange-red variety of medaka, *Oryzias latipes*) aged 8 weeks were used for most experiments. Fish were maintained at a stock level of 10 fish per tank in tap water with aeration. All 10 fish in a given tank received a daily ration of 200 mg of the diet prescribed for that group, and this was consumed completely within 14 h. All fish were maintained in accordance with the Animal Care Guidelines of Yamaguchi University. Medaka were divided into three groups: those fed HFD only (HFD group), control normal diet and those given HFD containing ezetimibe (HFD + ezetimibe group).

2.2. Diet

The proportions of protein, fat and carbohydrate, as well as the fatty acid compositions, of the control and HFD that were used in this study were as previously reported [8]. Ezetimibe was pulverized into a powder and mixed with HFD to give a dose of 0.01 mg per day, and was administered.

2.3. Histology

Euthanized fish were slit open from the anal vent to the gills, and the entire body was fixed with 4% paraformaldehyde in 0.1 M phosphate buffer (Muto, Tokyo, Japan). The liver was dissected, dehydrated in alcohol, and embedded in paraffin in accordance with standard procedures. Serial sections were cut and stained with hematoxylin and eosin (H&E). Liver macrophages were assessed by diastase-pas staining (DPAS staining). Five × 400-power fields were photographed in random locations on individual liver specimens stained with DPAS, and the number of DPAS-positive cells in each field was counted. In addition, a medaka NAFLD activity score (MNAS) [9] was determined based on human NAFLD activity score [10], and the tissue of individual livers was scored based on this. Trends in NASH severity were then quantitatively evaluated.

2.4. Blood analysis

Blood samples were analyzed as described [9]. Cholesterol and TG profiles in total lipoproteins were analyzed using a dual-detection HPLC system with two tandem-connected TSKgel Lipopropak XL columns (300 × 7.8 mm; Tosoh, Japan) by Skylight Biotech (Akita, Japan). The results were shown in Table 1A and B.

2.5. Measurement of triacylglycerol content and fatty acid in liver tissue

At 8 weeks after the start of the experiment, triacylglycerol content and fatty acid fractionation in liver tissue were measured in individual fish. Triacylglycerol in liver tissue was extracted using the method described by Folch et al. [11]. Fatty acids were methylated with boron trifluoride and methanol. Methylated fatty acids were analyzed as described [9].

Table 1
Blood lipid test results for the Control group, HFD 8 weeks group, and HFD + ezetimibe 8 weeks group (A and B). In each group, serum from 20 animals was collected and measurements were performed.

	Total	CM	VLDL	LDL	HDL
A					
Serum cholesterol concentration (mg/dL)					
Control	223.3	1.6	78.8	28.6	114.3
HFD 8 weeks	245.5	64.3	125.7	25.7	29.8
HFD + ezetimibe 8 weeks	132.0	21.7	62.3	13.8	34.1
B					
Serum triglyceride concentration (mg/dL)					
Control	509.6	6.6	248.5	45.2	209.4
HFD 8 weeks	2433.4	572.5	1187.7	265.2	408.0
HFD + ezetimibe 8 weeks	1202.5	202.4	553.2	94.1	352.8

2.6. Real-time RT-PCR analysis

Quantitative real-time RT-PCR was performed as described [12]. Primer sequences are listed in Supplementary information (Table S1).

2.7. Statistical analyses

Numerical data are expressed as means ± S.D. Student's *t*-test was performed in order to assess the statistical significance among the groups of medaka. *P* values less than 0.05 were considered to be significant.

3. Results

3.1. Changes in morphology, body weight and body mass index

On gross observations, abdominal distention (Fig. 1A) and whitish liver color (Fig. 1B) were seen in medaka of the HFD group. In the group given ezetimibe, abdominal distention improved (Fig. 1C) and liver color changed from white to dark red (Fig. 1D)(For interpretation of the references to colour in this figure legend, the reader is referred to the web version of this article.). Body length and body weight of each medaka were measured at the start of the experiment and after 4, 8, and 12 weeks on the respective diets. Body mass index (BMI) was calculated based on these measurements. In the HFD and HFD + ezetimibe groups, no differences were seen in changes in body weight or BMI throughout the entire experiment (Fig. 1E and F).

3.2. Ezetimibe ameliorated dyslipidemia in serum medaka NASH model

At 8 weeks after the start of the experiment, blood lipid tests were performed in the HFD and HFD + ezetimibe groups. The HFD group had higher total cholesterol and triacylglycerol levels than the Control group (total cholesterol: Control group, 223.3 mg/dl, HFD 8 weeks group, 245.5 mg/dl; triacylglycerols: Control group, 509.6 mg/dl, HFD 8 weeks group, 2433.4 mg/dl). Meanwhile, the HFD + ezetimibe group had lower total cholesterol and triacylglycerol levels than the HFD group (total cholesterol: HFD + ezetimibe 8 weeks group, 132.0 mg/dl; triacylglycerols: HFD + ezetimibe 8 weeks group, 1202.5 mg/dl) (Table 1). These results suggested that ezetimibe decreased high cholesteral and triacylglerol induced by HFD in serum.

3.3. Ezetimibe inhibited fatty acid accumulation in the liver in medaka NASH model

Next, the amount of fatty acid in the liver was measured, and at 8 weeks after the start of the experiment, the HFD group had

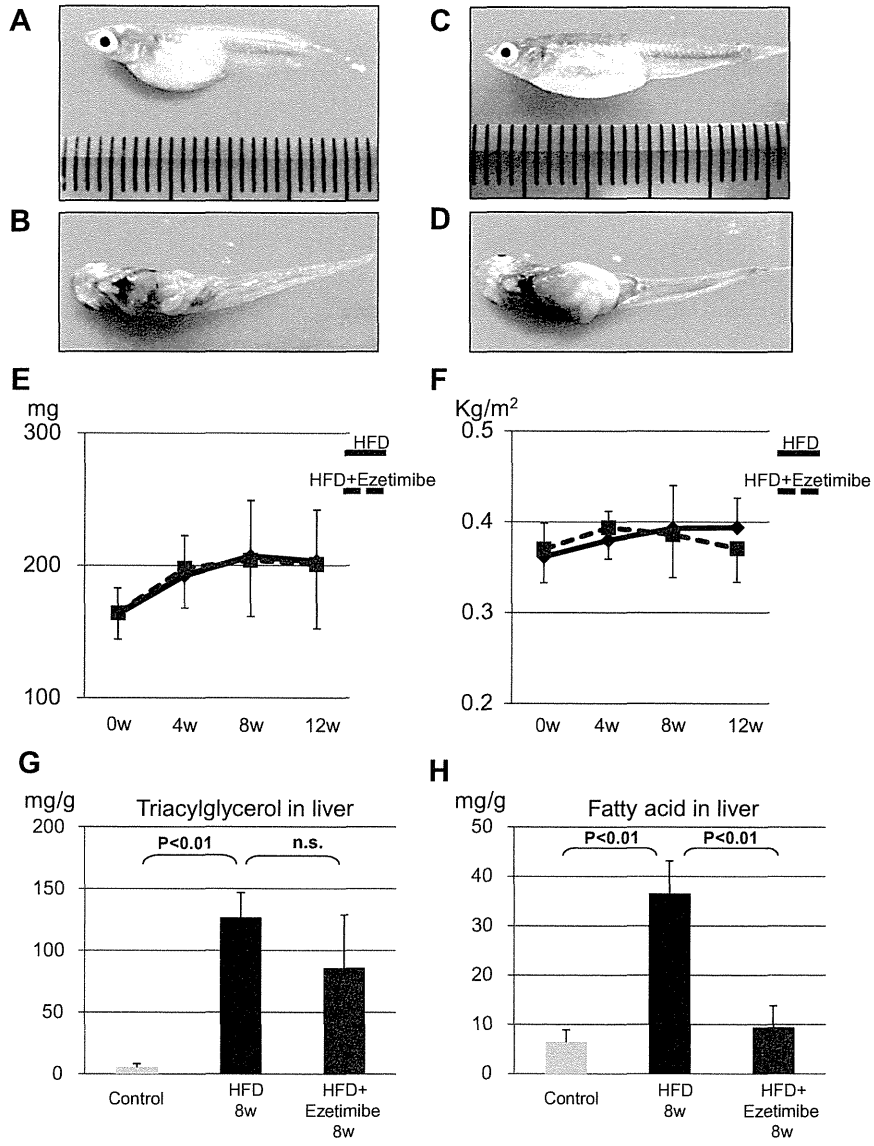

Fig. 1. Change in morphology after HFD for 12 weeks. Abdominal distension was observed (A). Liver showed a whitish color (B). Abdominal distention was reduced (C). Liver showed a brown color (D). Changes in body weight from the start to study completion in the HFD group and HFD + ezetimibe group (E). Change in body mass index from the start to study completion between the HFD group and HFD + ezetimibe group (F). Liver fat contents in the Control group, HFD 8 weeks group, and HFD + ezetimibe 8 weeks group (G). Liver fatty acid contents in the liver in the Control group, HFD 8 weeks group, and HFD + ezetimibe 8 weeks group (H). Data are means ± SD. n.s., no significant difference. (For interpretation of the references to colour in this figure legend, the reader is referred to the web version of this article.)

markedly higher triacylglycerol and fatty acid levels in the liver than the Control group (triacylglycerols: Control group, 5.5 ± 2.8 mg/g; HFD 8 weeks group, 126.6 ± 20.3 mg/g ($p < 0.01$); fatty acid: Control group, 6.5 ± 2.5 mg/g, HFD 8 weeks group, 36.5 ± 6.6 mg/g ($p < 0.01$), and the HFD + ezetimibe group had lower levels of liver fatty acid than the HFD group (liver fatty acid: HFD 8 weeks group, 36.5 ± 6.6 mg/g, HFD + ezetimibe 8 weeks group, 9.4 ± 4.3 mg/g ($p < 0.01$) (Fig. 1G and H).

3.4. Ezetimibe improved MNAS with decrease of infiltration of inflammatory cells in medaka NASH model

The HFD group had higher inflammatory cell infiltration in the liver at 8 and 12 weeks than the Control group (Control group, 0.6 ± 1.1/HPF, HFD 8 weeks group, 3.6 ± 3.0/HPF ($p < 0.01$), HFD 12 weeks group 7.9 ± 3.9/HPF ($p < 0.01$). At 4 and 12 weeks, the HFD + ezetimibe group showed inhibition of inflammatory cell infiltration in the liver, as compared to the HFD group (HFD 4 weeks group, 0.9 ± 1.6/HPF, HFD + ezetimibe 4 weeks group, 0.2 ± 0.6/HPF ($p < 0.05$); HFD 12 weeks group, 7.9 ± 3.9/HPF, HFD + ezetimibe 12 weeks group, 1.5 ± 2.2/HPF ($p < 0.01$) (Figs. 2, 3A).

3.5. Ezetimibe slowed progression of medaka NAFLD activity scores in medaka NASH model

The HFD group had significantly higher medaka NAFLD activity scores (MNAS) than the Control group at 8 and 12 weeks (Control group, 0.4 ± 0.5, HFD 8 weeks group, 4.0 ± 2.2 ($p < 0.05$), HFD 12 weeks group, 5.8 ± 1.5 ($p < 0.01$), while the HFD + ezetimibe group had significantly lower MNAS than the HFD group at 12 weeks (HFD 12 weeks group 5.8 ± 1.5, HFD + ezetimibe 12 weeks group, 2.0 ± 1.0 ($p < 0.05$) (Fig. 3B).

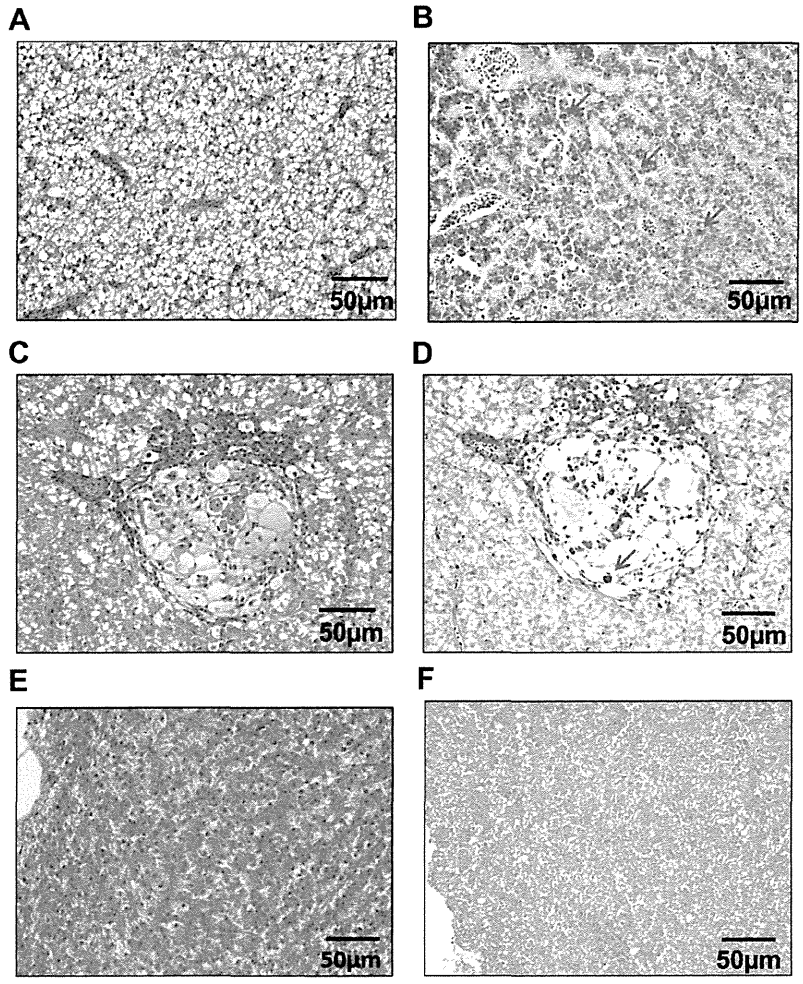

Fig. 2. Fat deposition in the liver at 8 weeks in the HFD. HE staining (A); DPAS-positive cells in the liver at 8 weeks in HFD (Arrow indicated). D-PAS staining (B); balloon-like changes in liver cells (C); DPAS-positive cells in this state (Arrow indicated) (D); liver after 8 weeks in the HFD + ezetimibe group (E); decreased fat deposition in the liver at 8 weeks (F). Measurements were performed in each ×400-power field. Data are means ± SD. n.s., no significant difference.

3.6. Changes in expression of lipid-related genes in liver

Investigation of lipid-related gene expression in liver revealed markedly decreased expression of PPAR alpha, AC03, MCAD, ACC1 and APoB in the group administered ezetimibe (Fig. 3C–I). These results indicated that gene related with fatty acid synthesis and oxidation were decreased.

4. Discussion

We previously developed and reported a medaka NASH model as an effective new model for drug screening for NASH [8]. The present study involved evaluation and analysis using ezetimibe in the medaka NASH model. Ezetimibe is a novel sterol absorption inhibitor that blocks Niemann–Pick C1-Like 1 (NPC1L1) – mediated cholesterol enterocytes [13]. It has already been reported, among other things, in animal experiments that ezetimibe improves dietary obesity [14,15], improves liver fatty change [14–17], and improves insulin resistance [16]. Using medaka NASH model, we also reported that telmisartan, which has angiotensin II type 1 receptor-inhibiting and PPAR-γ-stimulating actions, inhibits liver macrophage infiltration and inhibits the accumulation of liver fat, thereby improving the pathological condition of the medaka NASH model [9].

The effect of ezetimibe is quite different from telmisartan, In this study, however ezetimibe improved the abdominal distention caused by the high-fat diet and fat deposition in the liver (Fig. 1A–D), but ezetimibe did not produce major changes in BMI or body weight (Fig. 1E and F). However, ezetimibe decreased the amount of triacylglycerol and fatty acid in serum (Table 1A and B). Moreover the amount of fatty acid in the liver was significantly suppressed (Fig. 1G and H). When diagnosing the histopathological picture of NASH in humans, NAFLD activity score (NAS), which numerically quantifies the three factors of steatosis, inflammation and ballooning, is widely used [10]. We created the medaka NAFLD activity score (MNAS), and showed in analyses conducted with our medaka NASH model that the score increased as the pathological condition progressed with time. In recent studies, the increase in the number of macrophages infiltrating adipose tissue is reported to be related to obesity [18]. A comparative analysis of the HFD group and Control group looking only at inflammatory cells showed that, similar to MNAS, the number of inflammatory cells had increased after 8 and 12 weeks of HFD administration. These results indicated that inflammatory cells serve an important role in the progression of the NASH condition, (Fig. 2A–D), but ezetimibe group we could not find D-PAS positive cell (Fig. 2E and F). These results indicated that ezetimibe significantly inhibited the

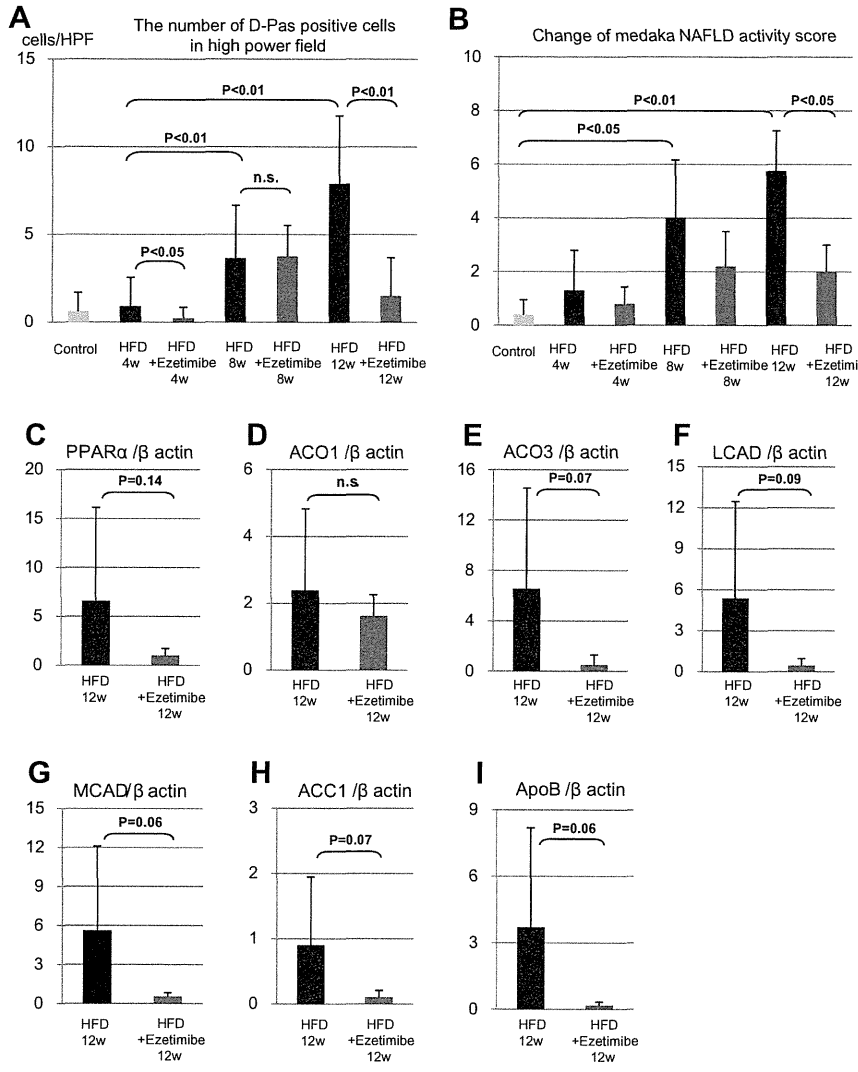

Fig. 3. Changes in DPAS-positive cells (A). Changes in MNAS (B). Trends in liver medaka NAFLD activity score in the HFD group and HFD + ezetimibe group. 4, 8 and 12 weeks data was presented. Scoring and quantification were performed for individual livers. Changes in gene expression of PPAR alpha (C), ACO1 (D), ACO3 (E), LCAD (F), MCAD (G), ACC1 (H) and ApoB (I) in the liver in the HFD group and HFD + ezetimibe group at 12 weeks.. Data are means ± SD. n.s., no significant difference.

infiltration of inflammatory cells in a medaka liver and MNAS was improved (Fig. 3A and B).

In medaka model, as shown in Fig. 3C–I, the amount of gene expression related to fat metabolism in liver tissue was decreased. Fatty acid synthesis and oxidation was decreased (Fig. 1H). Thus, ezetimibe administration was shown to decrease lipid synthesis activity in the liver. Numerous reports have ruled out the possibility that ezetimibe inhibits fatty acid absorption, although it has been reported that the expression of fatty acid transport protein 4 is decreased and fatty acid absorption is inhibited when NPC1L1 is knocked out in mice [19]. In addition, there have been no reports clarifying how fatty acids are absorbed in the small intestine of medaka. In this model, ezetimibe decreased the amount of triacylglycerol and fatty acid in serum and decreased the fatty acid in liver. This ezetimibe effect was quite effective for improvement of MNAS.

Moreover, according to a reported gene expression analysis in the liver of human NAFLD patients, the expression of genes related to fatty acid cleavage and fatty acid binding, lipolysis, macrophage migration and inflammation are elevated in NAFLD patients [20]. The infiltration of inflammatory cells, such as monocytes and macrophages, plays an important role in the progression of metabolic syndrome, and inflammatory cells are conjectured to serve important roles even in NASH, which is thought to be an expression of metabolic syndrome in the liver [18,21]. The present results confirmed an obvious decrease in inflammatory cells together with the decrease in the amount of fatty acid in the NASH liver. These results also showed that ezetimibe had an effect on anti-inflammation associated with metabolic syndrome.

In the present investigation, the results indicated that in the group administered ezetimibe, fat deposition in the liver was improved, and this was accompanied by an improvement in inflammation. Therefore, ezetimibe may have the potential to improve the inflammatory state that occurs in the body in association with metabolic syndrome.

In conclusion, we were able to observe the pathological changes resembling human NASH by administering a HFD to medaka. In this model, ezetimibe was effective in improving the pathological condition.

Acknowledgments

This study was supported by Grants-in-Aid for Scientific Research from the Japan Society for the Promotion of Science

(22659148, 23659398), the Japan Science and Technology Agency, and the Ministry of Health, Labour and Welfare.

Appendix A. Supplementary data

Supplementary data associated with this article can be found, in the online version, at http://dx.doi.org/10.1016/j.bbrc.2012.04.087.

References

[1] J. Ludwig, T.R. Viggiano, D.B. McGill, B.J. Oh, Nonalcoholic steatohepatitis: Mayo Clinic experiences with a hitherto unnamed disease, Mayo Clin. Proc. 55 (7) (1980) 434–438.
[2] C.P. Day, O.F. James, Steatohepatitis: a tale of two "hits"? Gastroenterology 114 (4) (1998) 842–845.
[3] P. Masahito, K. Aoki, N. Egami, T. Ishikawa, H. Sugano, Life-span studies on spontaneous tumor development in the medaka (*Oryzias latipes*), Jpn. J. Cancer Res. 80 (11) (1989) 1058–1065.
[4] M. Kasahara, K. Naruse, S. Sasaki, Y. Nakatani, W. Qu, B. Ahsan, T. Yamada, Y. Nagayasu, K. Doi, Y. Kasai, T. Jindo, D. Kobayashi, A. Shimada, A. Toyoda, Y. Kuroki, A. Fujiyama, T. Sasaki, A. Shimizu, S. Asakawa, N. Shimizu, S. Hashimoto, J. Yang, Y. Lee, K. Matsushima, S. Sugano, M. Sakaizumi, T. Narita, K. Ohishi, S. Haga, F. Ohta, H. Nomoto, K. Nogata, T. Morishita, T. Endo, T. Shin-I, H. Takeda, S. Morishita, Y. Kohara, The medaka draft genome and insights into vertebrate genome evolution, Nature 447 (7145) (2007) 714–719.
[5] K.C. Sadler, A. Amsterdam, C. Soroka, J. Boyer, N. Hopkins, A genetic screen in zebrafish identifies the mutants vps18, nf2 and foie gras as models of liver disease, Development 132 (15) (2005) 3561–3572.
[6] T. Watanabe, S. Asaka, D. Kitagawa, K. Saito, R. Kurashige, T. Sasado, C. Morinaga, H. Suwa, K. Niwa, T. Henrich, Y. Hirose, A. Yasuoka, H. Yoda, T. Deguchi, N. Iwanami, S. Kunimatsu, M. Osakada, F. Loosli, R. Quiring, M. Carl, C. Grabher, S. Winkler, F. Del Bene, J. Wittbrodt, K. Abe, Y. Takahama, K. Takahashi, T. Katada, H. Nishina, H. Kondoh, M. Furutani-Seiki, Mutations affecting liver development and function in Medaka, *Oryzias latipes*, screened by multiple criteria, Mech. Dev. 121 (7–8) (2004) 791–802.
[7] Y.S. Shieh, Y.S. Chang, J.R. Hong, L.J. Chen, L.K. Jou, C.C. Hsu, G.M. Her, Increase of hepatic fat accumulation by liver specific expression of Hepatitis B virus X protein in zebrafish, Biochim. Biophys. Acta 1801 (7) (2010) 721–730.
[8] T. Matsumoto, S. Terai, T. Oishi, S. Kuwashiro, K. Fujisawa, N. Yamamoto, Y. Fujita, Y. Hamamoto, M. Furutani-Seiki, H. Nishina, I. Sakaida, Medaka as a model for human nonalcoholic steatohepatitis, Dis. Model Mech. 3 (7–8) (2010) 431–440.
[9] S. Kuwashiro, S. Terai, T. Oishi, K. Fujisawa, T. Matsumoto, H. Nishina, I. Sakaida, Telmisartan improves nonalcoholic steatohepatitis in medaka (*Oryzias latipes*) by reducing macrophage infiltration and fat accumulation, Cell Tissue Res. 344 (1) (2011) 125–134.
[10] D.E. Kleiner, E.M. Brunt, M. Van Natta, et al., Design and validation of a histologic scoring system for nonalcoholic fatty liver disease, Hepatology 41 (2005) 1313–1321.
[11] J. Folch, M. Lees, Sloane Stanley GH. A simple method for the isolation and purification of total lipides from animal tissues, J. Biol. Chem. 226 (1) (1957) 497–509.
[12] T. Oishi, S. Terai, T. Iwamoto, T. Takami, N. Yamamoto, I. Sakaida, Splenectomy reduces fibrosis and preneoplastic lesions with increased triglycerides and essential fatty acids in rat liver cirrhosis induced by a choline-deficient L-amino acid-defined diet, Hepatol. Res. 41 (5) (2011) 463–474.
[13] S.W. Altmann, H.R. Davis, L.J. Zhu, X. Yao, L.M. Hoos, G. Tetzloff, et al., Niemann–Pick C1 Like 1 protein is critical for intestinal cholesterol absorption, Science 303 (2004) 1201–1204.
[14] M. Deushi, M. Nomura, A. Kawakami, M. Haraguchi, M. Ito, M. Okazaki, et al., Ezetimibe improves liver steatosis and insulin resistance in obese rat model of metabolic syndrome, FEBS Lett. 581 (2007) 5664–5670.
[15] E.D. Labonté, L.M. Camarota, J.C. Rojas, R.J. Jandacek, D.E. Gilham, J.P. Davies, et al., Reduced absorption of saturated fatty acids and resistance to diet-induced obesity and diabetes by ezetimibe-treated and Npc1l1−/− mice, Am. J. Physiol. Gastrointest. Liver Physiol. 295 (2008) 776–783.
[16] N. Assy, M. Grozovski, I. Bersudsky, S. Szvalb, O. Hussein, Effect of insulin-sensitizing agents in combination with ezetimibe, and valsartan in rats with non-alcoholic fatty liver disease, World J. Gastroenterol. 12 (2006) 4369–4376.
[17] S. Zheng, L. Hoos, J. Cook, G. Tetzloff, H. Davis Jr, M. van Heek, et al., Ezetimibe improves high fat and cholesterol diet-induced non-alcoholic fatty liver disease in mice Eur, J. Pharmacol. 584 (2008) 118–124.
[18] S.P. Weisberg, D. McCann, M. Desai, M. Rosenbaum, R.L. Leibel, A.W. Ferrante Jr., Obesity is associated with macrophage accumulation in adipose tissue, J. Clin. Invest. 112 (12) (2003) 1796–1808.
[19] E.D. Labonté, L.M. Camarota, J.C. Rojas, R.J. Jandacek, D.E. Gilham, J.P. Davies, Y.A. Ioannou, P. Tso, D.Y. Hui, P.N. Howles, Reduced absorption of saturated fatty acids and resistance to diet-induced obesity and diabetes by ezetimibe-treated and Npc1l1−/− mice, Am. J. Physiol. Gastrointest. Liver Physiol. 295 (4) (2008) G776–G783.
[20] J. Westerbacka, M. Kolak, T. Kiviluoto, P. Arkkila, J. Sirén, A. Hamsten, R.M. Fisher, H. Yki-Järvinen, Genes involved in fatty acid partitioning and binding, lipolysis, monocyte/macrophage recruitment, and inflammation are overexpressed in the human fatty liver of insulin-resistant subjects, Diabetes 56 (11) (2007) 2759–2765.
[21] M. Ishibashi, K. Hiasa, Q. Zhao, S. Inoue, K. Ohtani, S. Kitamoto, M. Tsuchihashi, T. Sugaya, I.F. Charo, S. Kura, T. Tsuzuki, T. Ishibashi, A. Takeshita, K. Egashira, Critical role of monocyte chemoattractant protein-1 receptor CCR2 on monocytes in hypertension-induced vascular inflammation and remodeling, Circ. Res. 94 (9) (2004) 1203–1210.

Cell Transplantation, Vol. 21, pp. 2363–2375, 2012
Printed in the USA.

0963-6897/12 $90.00 + .00
DOI: http://dx.doi.org/10.3727/096368912X638856
E-ISSN 1555-3892
www.cognizantcommunication.com

Granulocyte Colony-Stimulating Factor and Interleukin-1β Are Important Cytokines in Repair of the Cirrhotic Liver After Bone Marrow Cell Infusion: Comparison of Humans and Model Mice

Yuko Mizunaga,* Shuji Terai,* Naoki Yamamoto,* Koichi Uchida,* Takahiro Yamasaki,* Hiroshi Nishina,† Yusuke Fujita,‡ Koh Shinoda,§ Yoshihiko Hamamoto,‡ and Isao Sakaida*

*Department of Gastroenterology and Hepatology, Yamaguchi University Graduate School of Medicine, Yamaguchi, Japan
†Department of Developmental and Regenerative Biology, Medical Research Institute, Tokyo Medical and Dental University, Tokyo, Japan
‡Department of Computer Science and Systems Engineering, Faculty of Engineering, Yamaguchi University, Yamaguchi, Japan
§Department of Neuroanatomy and Neuroscience, Yamaguchi University School of Medicine, Yamaguchi, Japan

We previously described the effectiveness of autologous bone marrow cell infusion (ABM*i*) therapy for patients with liver cirrhosis (LC). We analyzed chronological changes in 19 serum cytokines as well as levels of specific cytokines in patients after ABM*i* therapy and in a mouse model of cirrhosis generated using green fluorescent protein (GFP)/carbon tetrachloride (CCl_4). We measured expression profiles of cytokines in serum samples collected from 13 patients before and at 1 day and 1 week after ABM*i*. Child–Pugh scores significantly improved in all of these patients. To analyze the meaning of early cytokine change, we infused GFP-positive bone marrow cells (BMCs) into mice with CCl_4-induced LC and obtained serum and tissue samples at 1 day and as well as at 1, 2, 3, and 4 weeks later. We compared chronological changes in serum cytokine expression in humans and in the model mice at 1 day and 1 week after BMC infusion. Among 19 cytokine, both granulocyte colony-stimulating factor (G-CSF) and interleukin-1β (IL-1β) in serum was found to show the same chronological change pattern between human and mice model. Next, we examined changes in cytokine expression in cirrhosis liver before and at 1, 2, 3, and 4 weeks after BMC infusion. Both G-CSF and IL-1β were undetectable in the liver tissues before and at 1 week after BMC infusion but increased at 2 weeks and continued until 4 weeks after infusion. The infused BMCs induced an early decrease of both G-CSF and IL-1β in serum and an increase in the model mice with LC. These dynamic cytokine changes might be important to repair liver cirrhosis after BMC infusion.

Key words: Autologous bone marrow infusion (ABM*i*); Cytokine; Liver regeneration; Cell therapy; Chronological change

INTRODUCTION

Liver transplantation is presently the only radical therapy for liver failure, but the scarcity of donors and highly invasive surgery remain formidable obstacles. Cells in the bone marrow might differentiate into hepatocytes was reported (1,23,24). This suggested that bone marrow could serve as a new source of cells to regenerate the liver of patients with liver cirrhosis (LC) (22). To develop autologous bone marrow cell (BMC) infusion (ABM*i*) therapy, we analyzed the effects of green fluorescent protein (GFP)-positive BMC infusions into carbon tetrachloride (CCl_4)-induced cirrhosis mouse model (GFP/CCl_4 model) (20,21). From this GFP/CCl_4 model, we found that liver function, fibrosis, and survival rates were improved by BMC infusion (15,18–21). From these basic studies of the GFP/CCl_4 model, we therefore developed ABM*i* therapy and have clinically applied it to treat LC since 2003. We reported that liver function obviously improved in nine patients in terms of total protein, serum albumin, and Child–Pugh scores after 6 months of long-term follow-up (18). Furthermore, long-term follow-up clarified the value of ABM*i* (22). Since then, clinical studies have verified our findings regarding the effectiveness of ABM*i* therapy (18), and others have also reported that ABM*i* therapy is effective against liver cirrhosis in patients (8,14,17). Recently,

Received August 23, 2010; final acceptance January 15, 2012. Online prepub date: April 10, 2012.
Address correspondence to Shuji Terai, M.D., Ph.D., Associate Professor, Department of Gastroenterology and Hepatology, Yamaguchi University Graduate School of Medicine, Minami Kogushi 1-1-1, Ube, Yamaguchi 755-8505, Japan. Tel: +81-836-22-2240; Fax: +81-836-22-2303; E-mail: terais@yamaguchi-u.ac.jp

the effectiveness of autologous bone mesenchymal stem cell transplantation into liver failure patient was also reported (13).

Several recent reports have described the therapeutic effects of BMC transplantation upon nonneoplastic conditions such as autoimmune diseases, ischemic heart disease, and heart failure (4,5), and that cytokines might be involved in tissue repair and cell differentiation. However we previously analyzed a molecular analysis for GFP/CCl_4 model using DNA chips to identify molecules and factors involved in local liver regeneration after bone marrow cell infusion (12), but the expression profiles of cytokines in serum have not been confirmed. The present study examines changes in the early expression profiles of serum cytokines that have so far been impossible to determine in human and mice model. We investigated chronological changes in serum cytokines that are associated with the ability of infused BMCs to repair the liver of patients with LC. Serum cytokines were comprehensively measured, and chronological changes in their expression were compared between serum samples from patients and from the mouse GFP/CCl_4 model mice to determine the kinetics of those involved in liver repair induced by BMCs. We calculated logarithms and corrected individual differences for comparisons to define only the degree of chronological change at each time phase for individual cytokines.

Thus, instead of differences among simple measurements, we determined chronological changes in cytokine kinetics and investigated differences to identify target cytokines. We extracted target serum markers by comparing degrees of chronological change in several cytokines in multiple dimensions after BMC infusion. We then analyzed candidate cytokines that were important for repairing the cirrhotic liver after BMC infusion.

MATERIALS AND METHODS

ABMi Therapy Protocol

Eligible patients were aged between 18 and 75 years and clinically diagnosed with LC. We enrolled those with LC with total bilirubin (T. Bil) < 3.0 mg/dl, platelets (Plt) < 5 (10^{10}/L), and no visible hepatocellular carcinoma on computed tomography (CT) or magnetic resonance images. Patients were excluded if their conditions also involved organs other than the liver, such as the heart or lungs. Data are from patients who were followed up for 6 months. The protocol was the same as that in our previous study (17). To date, 19 patients have undergone ABM*i* for LC, and no major adverse effects have been identified in Yamaguchi University. Among 19 patients, we could analyze serum cytokine for 13 patients (Table 1) of whom we were able to follow their progress with sufficient samples. All protocols were approved by the ethics committee of Yamaguchi University, and written informed consent was obtained from all patients to participate in the study.

Statistical Analysis

The changes in laboratory data (Child–Pugh score) from baseline (before BMC infusion) to 1 or 6 months after the BMC infusion were analyzed. Values are shown as means ± SE. Data were analyzed using an analysis of variance with Fisher's projected least significant difference test.

GFP/CCl_4 Model

C57BL6/Tg14 (act-enhanced GFP) OsbY01 mice (GFP-Tg mice) expressing GFP in various tissues and cells were provided by Masaru Okabe (Genome Research Center, Osaka University, Osaka, Japan) (11). Six-week-old female C57BL/6 mice (Japan SLC, Shizuoka, Japan) were intraperitoneally injected with 0.5 ml CCl_4/kg body weight twice each week for 4 weeks to induce persistent LC. Immediately after 4 weeks of CCl_4 administration, 1×10^5 GFP-positive BMCs were injected into the tail vein (15,21). The BMCs were obtained from GFP-Tg mice as follows. The limbs were removed from sacrificed GFP-positive mice, and then BMCs were flushed from the medullary cavities of the tibias and femurs using a 25-gauge needle containing PBS culture medium. The GFP-positive bone marrow cells were previously shown to express one or more of CD11b, CD44, and CD90 (6,15). The same dose of CCl_4 was injected twice each week after BMC infusion. Individual mice were killed at 24 h after the initial CCl_4 injection and once each week after the BMC infusion for 4 weeks. All procedures including surgical steps proceeded in accordance with the guidelines for experiments involving animals and recombinant DNA at Yamaguchi University.

Expression Profiles of Cytokines Determined Using Bio-Plex Suspension Arrays (Human and Mouse Sera)

Human study: We obtained serum from 13 patients with LC before and at 1 day and 1 week after starting ABM*i* therapy. Model mouse study: Mice were continuously injected with CCl_4 after the BMC infusion. We then measured concentrations of interleukin (IL)-1β, IL-2, IL-4, IL-5, IL-6, IL-10, IL-12(p70), IL-13, IL-17, granulocyte colony-stimulating factor (G-CSF), granulocyte macrophage colony-stimulating factor (GM-CSF), fibroblast growth factor (FGF)-basic, interferon-γ (IFN-γ), monocyte chemoattractant protein (MCP)-1, macrophage inflammatory protein (MIP)-1α, MIP-1β, regulated upon activation T-cell expressed and secreted (RANTES), tumor necrosis factor α (TNF-α), and vascular endothelial growth factor (VEGF) in duplicate in at least 11 samples of mouse serum collected at 1 day and 1 week after BMC

Table 1. Patients' Characteristics

Patient No.	Age (years)	Gender	Etiology	Child–Pugh Score	Medication/Therapy (per day)
1	69	M	HBV	9	AminolebanEN 1 pack Livact 3 packs Furosemide 40 mg
2	59	M	HBV	8	Livact 3 packs/day
3	69	M	HCV	8	AminolebanEN 1 pack Furosemide 80 mg Spironolactone 50 mg
4	63	M	HCV	9	AminolebanEN 2 packs Furosemide 30 mg Spironolactone 50 mg
5	60	M	HCV	9	AminolebanEN 2 packs Spironolactone 25 mg
6	61	M	HCV	9	Livact 3 packs Spironolactone 25 mg
7	58	M	HCV	7	Livact 3 packs Furosemide 20 mg
8	62	F	HCV	6	Livact 3 packs Furosemide 20 mg
9	62	F	HCV	7	Livact 3 packs Furosemide 20 mg Spironolactone 25 mg
10	67	M	HCV	11	Furosemide 20 mg Spironolactone 25 mg
11	73	M	HCV	8	–
12	54	M	HCV	9	Furosemide 20 mg Spironolactone 50 mg
13	69	F	HCV	7	Spironolactone 25 mg
Median	63.5			8.2	

M, male; F, female; HBV, hepatitis B virus; HCV, hepatitis C virus.

infusion. Concentrations of all tested cytokines were simultaneously evaluated using multiplex bead-based sandwich immunoassay kits (mouse and human 19-plex; Bio-Rad Laboratories, Tokyo, Japan) according to the manufacturer's instructions. In brief, 19 distinct sets of fluorescently labeled beads were loaded with capture monoclonal antibodies specific to each tested cytokine. Samples or standards (both 50 μl/well) were incubated with 50 μl of premixed bead sets in wet 96-well microtiter plates. The plates were washed, 25 μl of fluorescent detection antibody mixture was added for 30 min, the plates were washed again, and the samples were resuspended in assay buffer (Bio-Rad Laboratories, Tokyo, Japan). Standard curves for each soluble factor ranged from 0.2 to 3,200 pg/ml. The formation of different sandwich immunocomplexes on distinct bead sets was quantified using the Bio-Plex Suspension Array System (Bio-Rad Laboratories, Tokyo, Japan). Fluorescent signals from ≥100 beads per region (chemokine/cytokine) in 50-μl samples from each well were evaluated. Values with a coefficient of variation (CV) of >10% were discarded before the final data analysis.

Cytokine Data Analysis

Cytokine data from human ABM*i* samples (13 cases) and mouse samples for each time point ($n=11$ per time point) were analyzed using Bio-Plex Manager software version 3.0 (Bio-Rad Laboratories).

Analysis of Chronological Changes in Serum Cytokines From Humans After ABMi and From Model Mice

The concentrations of 19 cytokines at each time point were measured in all human and mouse serum samples using the Bio-Plex suspension array system.

Serum was separated from blood samples collected from patients before and at 1 day, 1 week, and 1 month after ABM*i*. Serum and liver tissue samples were collected from model mice before isogenic GFP-positive BMC infusion and during the early phase (1 day and 1 week after infusion). The degree of chronological changes in the cytokines before and after BMC infusion was determined in all serum samples.

The results from each cytokine generated from serum samples of the 13 treated patients were analyzed as follows based on the assumption of normal distribution.

Firstly, cytokine values considered as outliers were removed based on mean and standard deviation information. Secondly, we used the logarithm function representing the degree of change in each cytokine between two consecutive time points such as from before to 1 day or from 1 day to 1 week after ABM*i* therapy to determine degrees of chronological changes (12). The value of the logarithm function indicates the degree of chronological changes in one cytokine, which becomes the axis value of the corresponding cytokine. Finally, we found cytokines with similar chronological changes between the two models and/or larger chronological changes. Means (μ) and standard deviation (SD) were calculated, and values outside μ (means) ± 2SD were excluded. The means for each of the 19 cytokines before and 1 day and 1 week after ABM*i* therapy are defined as x_1, x_2, and x_3, respectively, in each of the 13 serum samples collected from patients.

Using the same method for the model mouse samples ($n=11$ per time point), x is defined as the average value for each of the 19 cytokines at each time point for the group infused with BMC, and x_1, x_2, and x_3 are defined as before and 1 day and 1 week after BMC infusion, respectively.

The degrees of chronological changes in each cytokine from before to 1 day after (f_1) and from 1 day after to 1 week after BMC infusion (f_2) were calculated as follows:

$$f_i=\log_2(x_{i+1}/x_i),\ i\text{: 1, 2 and the base of logarithm: 2.}$$

When $x_{i+1}=x_i$, the value of f becomes 0. That is, the value of f represents the degree of chronological change of a cytokine. Visualization by vector representation allows effective focus on the degree of change in cytokines between two consecutive time points.

Vector (F_j) comprising f_1 and f_2 was defined as follows to represent chronological changes in cytokine j:

$$F_j=[f_1, f_2].$$

The degree of chronological changes in cytokines for the BMC infusion group is displayed in a two-dimensional plane. In general, as the norm of the above vector F_j increases, the degree of chronological changes in cytokines also increases. Moreover, the distance between cytokines with similar chronological changes in the two-dimensional plane is less than that between cytokines with different chronological changes. Therefore, we examined cytokines with similar chronological changes and extracted those with similar changes between patients and model mice. $F(h)_j$ and $F(m)_j$ (where $j=1, \ldots, 19$) respectively indicate vectors for a chronological change in cytokine j in the patients and in the mouse model.

The time courses of chronological changes in 19 cytokines for the patients who received ABM*i* and for the model mice infused with BMCs were analyzed, and correlations were further investigated (Fig. 1A).

Comparison of Cytokines in Control Model Mice (Injected Only With CCl_4) and Those Infused With BMCs

We examined cytokines with synchronized chronological changes in the ABM*i* model and CCl_4 control model. Serum cytokines were compared at the same time points in the mice that were infused with BMCs and those that received only CCl_4 to determine whether levels changed with the BMC infusion.

The mice that received CCl_4 for 4 weeks were randomly divided into two groups (Fig. 1B). One group was infused with BMCs (GFP/CCl_4 model), and the other continued to receive CCl_4 twice weekly without BMC infusion (control). We defined X_1 as the time point before the BMC infusion and X'_1 as the same time in control group before the BMC infusion on Figure 1B. We defined X_2 as the time point at 1 day after BMC infusion and X'_2 as the same time as X_2 in the control group. We examined chronological changes in the patients and in two models of mice until 1 week after BMC infusion. Thus, X_3 and X'_3 were defined as the time points at 1 week after BMC infusion and as the same time point as X_3 in the control group, respectively ($n \geq 10$ per group). We simultaneously compared serum concentrations of cytokines extracted from each group and X'_2 with X_2, and X_3 and X'_3 using a t test.

Imunohistochemical Staining of Model Mouse Liver Tissue

We investigated G-CSF and IL-1β expression in 4-μm sections of paraffin-embedded blocks of mouse liver samples by immunohistochemical staining using the standard avidin–biotin–peroxidase complex (ABC) method. Sections were dewaxed in xylene, dehydrated in a graded alcohol series, and heated in a microwave oven for 6 min to activate antigens. Endogenous peroxidase activity was blocked by immersing the sections for 30 min in 0.3% hydrogen peroxidase in methanol. The sections were washed with distilled water, incubated in PBS containing rabbit serum for 20 min to block nonspecific antibody binding, and then incubated with goat anti-mouse G-CSF (diluted 1:300; Santa Cruz Biotechnology) and goat anti-mouse IL-1β (diluted 1:300; Santa Cruz Biotechnology) antibodies overnight at 4°C. The sections were incubated with biotin-conjugated secondary antibody in PBS for 60 min at room temperature and reacted with ABC for 30 min. Positive reactions were developed for about 3 min in PBS containing hydrogen peroxidase and 3,3′-diaminobenzidine (DAB). We captured five areas (200×) and calculated G-CSF and IL-1β-positive expression rates at each time point (before and 1–4 weeks after the BMC infusion). Values are shown as mean ± SD. Data were analyzed with the ANOVA with PLSD test. A value of $p<0.05$ was considered statistically significant.

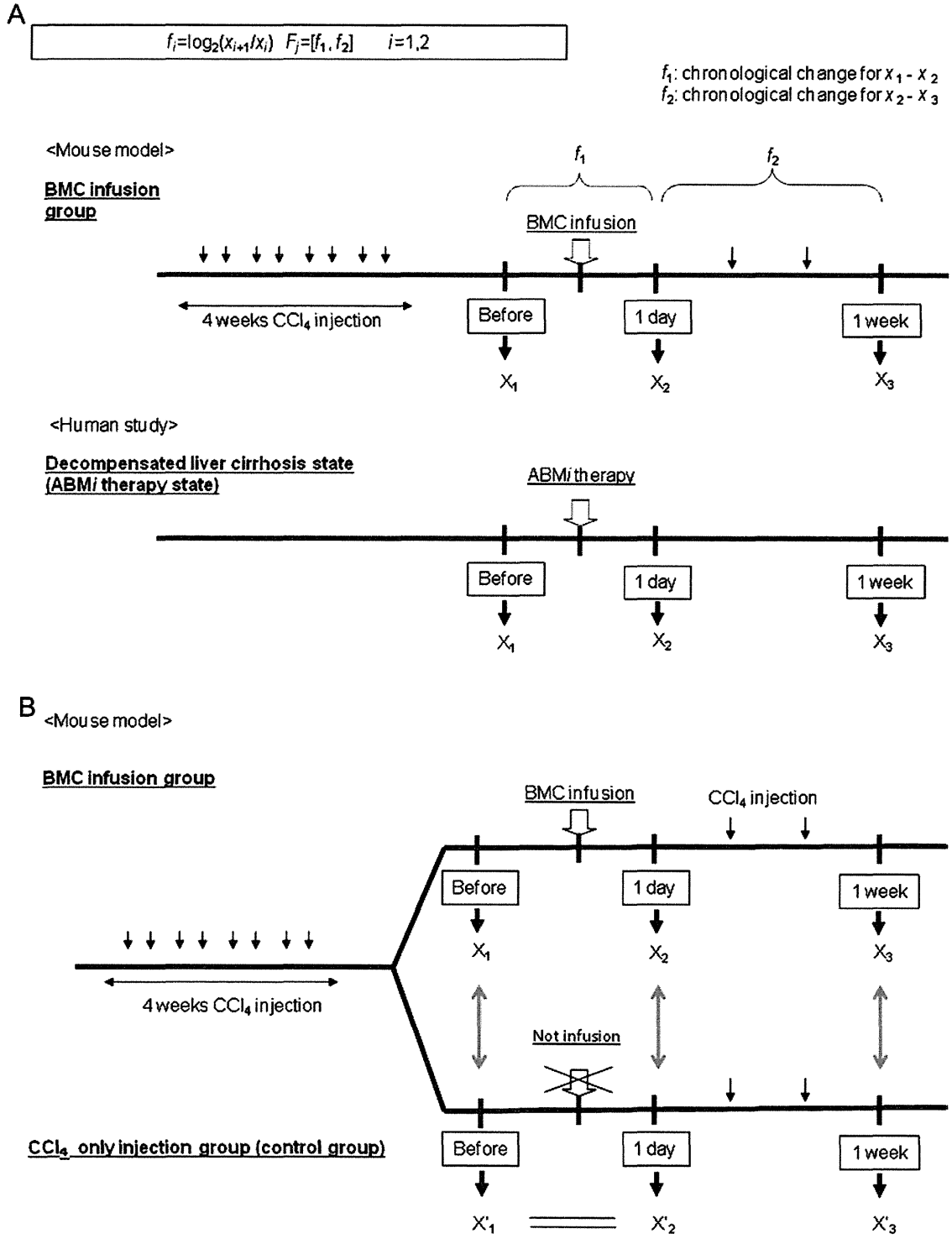

Figure 1. Definition of cytokine measurement points in patients and in model mice. (A) Chronological changes in each cytokine from before to 1 week after (f_1) and from 1 day to 1 week after (f_2) bone marrow cell (BMC) infusion were calculated as $f_i=\log_2(x_{i+1}/x_i)$, i: 1,2, and base of logarithm: 2. Vectors comprising f_1 and f_2(F) are defined as $F_j=[f_1, f_2]$ to investigate chronological changes in each cytokine. ABMi, autologous bone marrow cell infusion; CCl_4, carbon tetrachloride. (B) Comparison between the control group (CCl_4) and BMC infusion group. Model mice received (CCl_4) for 4 weeks and were then randomly assigned to either a group that continued to receive only CCl_4 twice weekly (control) or another that was infused with BMCs as green fluorescent protein (GFP)/CCl_4. We defined X_1 as the time point before the BMC infusion and X'_1 as the same time in control group before the BMC infusion on (B), each time point in each group was defined as X_2: 1 day after BMCs and X'_2: same time as X_2 in the control group. Similarly, X_3: 1 day after BMCs and X'_3: same time as X_3 in control group.

RESULTS

ABMi Therapy Improved Liver Function in 13 Patients

Therapy with ABM*i* continued, and the present study examined for total of 13 patients (Table 1). Child–Pugh scores (Fig. 2) showed that liver function improved after ABM*i* therapy ($p<0.05$).

Changes in Serum Cytokines in Patients After ABMi

Figure 3A plots the chronological changes in each cytokine from the patients on a two-dimensional plane. The x component of a vector from the origin to a plotted point (f_1) indicates chronological changes from before to 1 day after BMC infusion, and the y component (f_2) indicates chronological changes from 1 day to 1 week after infusion. The quadrant of each vector and the magnitude (distance) of each vector $[\sqrt{(|f_1|^2+|f_2|^2)}]$ are presented. A larger distance between vectors means a greater difference in the degree of change over time for the patients. Table 2 shows that, among the 19 human cytokines, the distance between time points was the greatest for G-CSF>IL-6>IL-1β (3.3119, 2.2181, and 1.2531, respectively), confirming differences in degrees of chronological change. Human G-CSF (F_j), IL-6, and IL-1β were located in quadrants 2, 4, and 2, respectively.

Comparison Between Patients and Model Mice

We plotted f_1 on the x-axis and f_2 on the y-axis and indicated chronological changes in cytokine levels in patient and model mouse sera as vectors on the x–y plane, as shown in Figure 3B. Cytokines with large differences in degrees of chronological change at each time point were examined and those with similar chronological changes between the patients and mice were identified.

Vectors were also calculated for the GFP/CCl_4 model mice, and Table 3 shows the results along with data from the patients, which allows straightforward comparisons of changes in each cytokine between the two. Thus, we could identify important factors involved in liver regeneration after BMC infusion.

Cytokines between two models with similar chronological changes were plotted on a two-dimensional plane to calculate the magnitude of vectors for each cytokine in each model. If vectors for both models were found in the same quadrant, then we assumed identical kinetic chronological changes for that cytokine.

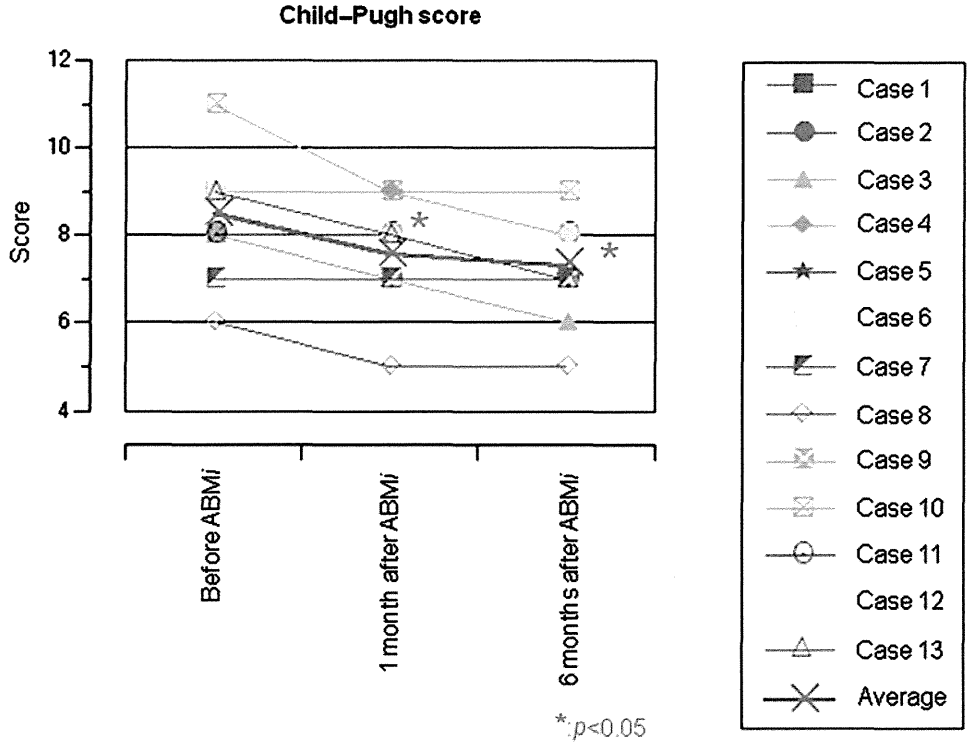

Figure 2. Evaluation of liver function in 13 patients after autologous bone marrow cell infusion (ABM*i*). Child–Pugh scores indicate significantly improved liver function at 1 and 6 months after ABM*i* compared with before (*$p<0.05$).

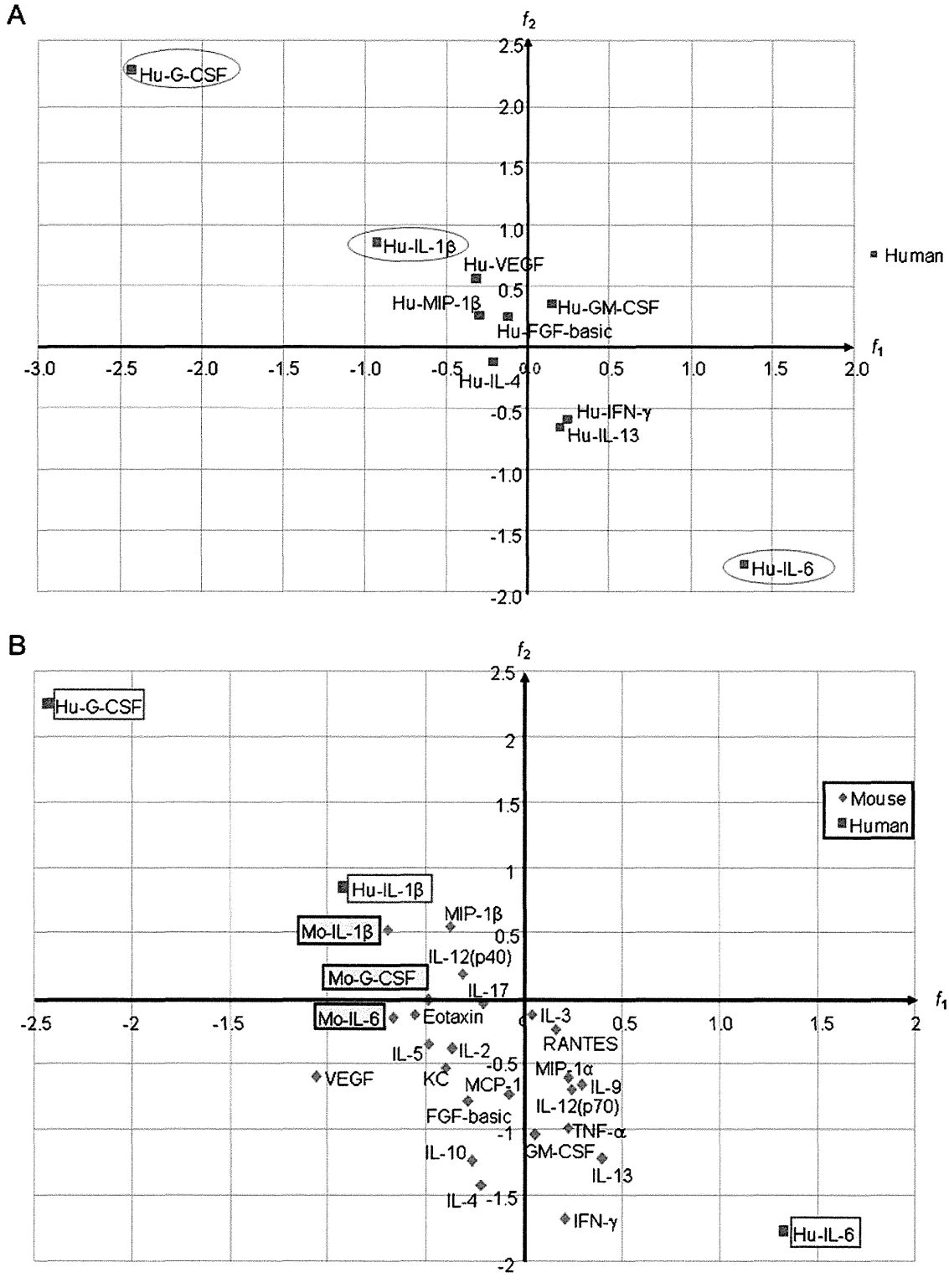

Figure 3. (A) Two-dimensional vector representation of chronological changes in human cytokines. Degrees of chronological changes in human cytokines are plotted on two-dimensional plane. Degree of chronological change from before to 1 day after BMC infusion is indicated as x component of vector from origin to a plotted point (f_1); that from 1 day to 1 week after infusion is indicated as y component (f_2). Quadrant and magnitude (distance) of each vector [$\sqrt{(|f_1|^2+|f_2|^2)}$] are shown. (B) Comparison of chronological changes in human and mouse G-CSF, IL-1β, and IL-6. Infusion with BMCs exerted significantly different chronological changes in human G-CSF, IL-1β, and IL-6 expression. These fluctuations are compared with those in mice by two-dimensional vector representation. Yellow and white boxes, mouse (M) and human (H) values, respectively. G-CSF, granulocyte colony-stimulating factor; IL, interleukin.

Table 2. Specific Cytokines in Patients After ABM*i*

	Human $F(h)_j$			
Human Cytokine	f_1	f_2	Quadrant	Vector Magnitude
G-CSF	–2.4287	2.2516	2	3.3119
IL-6	1.3305	–1.7747	4	2.2181
IL-1β	–0.9222	0.8484	2	1.2531
MIP-1α	0.3429	–0.8326	4	0.9004
IL-13	0.2023	–0.6583	4	0.6887
IFN-γ	0.2492	–0.5971	4	0.6470
VEGF	–0.3146	0.5521	2	0.6355
IL-12(p70)	–0.4281	0.1504	2	0.4537
MIP-1β	–0.2894	0.2531	2	0.3845
GM-CSF	0.1542	0.3453	1	0.3782
RANTES	–0.1275	0.3248	2	0.3490
IL-10	0.1694	–0.2668	4	0.3161
FGF-basic	–0.1191	0.2437	2	0.2712
IL-4	–0.2107	–0.1227	3	0.2438
IL-2	–0.1960	–0.1164	3	0.2279
IL-17	–0.1996	–0.0065	3	0.1997
TNF-α	–0.0170	–0.1838	3	0.1846
IL-5	0.1300	–0.0905	4	0.1584
MCP-1	–0.0604	–0.1179	3	0.1325

G-CSF, granulocyte colony-stimulating factor; IL, interleukin; MIP, macrophage inflammatory protein; IFN, interferon; VEGF, vascular endothelial growth factor; GM-CSF, granulocyte macrophage colony-stimulating factor; RANTES, regulated upon activation, T-cell expressed and secreted; FGF, fibroblast growth factor; TNF, tumor necrosis factor; MCP, monocyte chemotactic protein.

Analysis of G-CSF, IL-1β, and IL-6

Chronological changes in human G-CSF, IL-1β, and IL-6 expression significantly differed after BMC infusion, so we investigated their time course in the model mice.

Model mouse IL-1β lay in quadrant 2, and G-CSF lay on the *x*-axis at the borderline between quadrants 2 and 3. The two human cytokines also plotted in quadrant 2, thus suggesting that chronological changes after BMC infusion were the same in humans and mice. However, human and mouse IL-6 lay in quadrants 4 and 3, respectively. Thus, the profiles of chronological changes in human and mouse G-CSF and IL-1β were identical, whereas those of IL-6 were not.

Both human and model mouse G-CSF and IL-1β lay in quadrant 2, where the vectors indicated a "decrease" in f_1 and an "increase" in f_2. The two-dimensional vector for G-CSF was primarily located on the *x*-axis, thus clarifying that the chronological change from before to 1 day after BMC infusion was negative and that the degree of change tended to decrease. The chronological change was small from 1 day to 1 week after infusion. Levels of human and mouse IL-1β decreased from before to 1 day after but increased from 1 day to 1 week after BMC infusion (Fig. 3B). Thus, the comparable chronological changes in serum G-CSF and IL-1β in humans and mice suggested a high degree of similarity between the two models.

Comparison of G-CSF and IL-1β Between Model Mice Injected With CCl_4 (Control) and Those Injected With CCl_4 and Infused With BMC

Both G-CSF and IL-1β chronologically changed in a synchronized fashion in the GFP/CCl_4 mouse model and in the patients after ABM*i*. We compared the concentration of each cytokine in the control mice and the BMC-infused mice at the same time point (1 day and 1 week after BMC infusion) to determine whether the BMC infusion altered cytokine concentrations. In addition, we performed the *t* test on two groups, control group (X_1') and the group before the BMC infusion (X_1) on Figure 1B, and we confirmed that there is no significant difference between the two groups, which they divided at random, X_1' and X_1. We defined the two groups, X_1' and X_1, as equal groups (Fig. 4a, b). We thought that the difference between the two groups (control group and BMC group) from before BMC infusion to 1 day after BMC infusion is due to the BMC infusion. And since the time from X_1' to X_2' in the control group is only a day, we thought that each group at these two time points are approximately equal groups. We measured serum levels of each cytokine in two groups

Table 3. Similarity of Specific Cytokines in Patients and GFP/CCl_4 Model Mice

Human $F(h)_j$			Mouse $F(m)_j$			Human–Mouse	
Cytokine	f_1	f_2	Cytokine	f_1	f_2	Distance Between Vectors	Quadrant
IL-17	−0.1996	−0.0065	IL-17	−0.2059	−0.0384	0.0325	° 3
MIP-1α	0.3429	−0.8326	MIP-1α	0.2296	−0.6016	0.2573	° 4
MIP-1β	−0.2894	0.2531	MIP-1β	−0.3760	0.5482	0.3075	° 2
IL-2	−0.1960	−0.1164	IL-2	−0.3625	−0.3845	0.3156	° 3
IL-1β	−0.9222	0.8484	IL-1β	−0.6928	0.5160	0.4039	° 2
IL-13	0.2023	−0.6583	IL-13	0.4010	−1.2143	0.5905	° 4
MCP-1	−0.0604	−0.1179	MCP-1	−0.0762	−0.7288	0.6111	° 3
IFN-γ	0.2492	−0.5971	IFN-γ	0.2111	−1.6748	1.0783	° 4
IL-4	−0.2107	−0.1227	IL-4	−0.2206	−1.4229	1.3002	° 3
G-CSF	−2.4287	2.2516	G-CSF	−0.4817	−0.0077	2.9825	° 2
IL-12(p70)	−0.4281	0.1504	IL-12(p70)	−0.2821	−0.0988	0.2888	
RANTES	−0.1275	0.3248	RANTES	0.1634	−0.2337	0.6298	
IL-5	0.1300	−0.0905	IL-5	−0.4830	−0.3512	0.6661	
TNF-α	−0.0170	−0.1838	TNF-α	0.2263	−0.9883	0.8405	
FGF-basic	−0.1191	0.2437	FGF-basic	−0.2857	−0.7817	1.0389	
IL-10	0.1694	−0.2668	IL-10	−0.2616	−1.2358	1.0605	
VEGF	−0.3146	0.5521	VEGF	−1.0580	−0.5955	1.3673	
GM-CSF	0.1542	0.3453	GM-CSF	0.0555	−1.0354	1.3843	
IL-6	1.3305	−1.7747	IL-6	−0.6642	−0.1497	2.5729	

The circles indicate that the two vectors $F(h)_j$ and $F(m)_j$, which correspond to a cytokine j, are located in the same quadrant. This means that, in the cytokine, the chronological change pattern of human and mouse are the same.

at each point using the t test. Serum concentrations of G-CSF and IL-1β in the BMC-infused group at 1 day after BMC infusion and in the control group tended to decrease with a significant difference ($p<0.05$) (Fig. 4c, d) but did not significantly differ at 1 week after BMC infusion (Fig. 4e, f).

G-CSF and IL-1b Expression on Mouse Liver Tissue After BMC Infusion

Although the key factors involved in the liver repair mechanism of BMC infusion were identified, therefore, we immunostained liver tissues to investigate the expression of G-CSF and IL-1β, which might be regulated at the early phase after BMC infusion. Liver tissues from model mice apparently did not express G-CSF before and at 1 week after BMC infusion, but the ratio of the stained area was significantly greater at 2 weeks thereafter (Fig. 5a–e). The rates of expression became relatively stable and were significantly higher at 2, 3, and 4 weeks after BMC infusion than before and at 1 week thereafter ($p<0.01$) (Fig. 5f). The results were the same for IL-1β (Fig. 6a–e) ($p<0.01$) (Fig. 6f).

DISCUSSION

Here, we comprehensively compared chronological changes in serum cytokines after BMC infusion between humans and mice and clarified the importance of early-phase changes in the kinetics of G-CSF and IL-1β, both of which are involved in liver regeneration.

To the best of our knowledge, the present study is the first to comprehensively measure chronological changes in cytokines during liver repair after BMC infusion in humans and mice. Substantial differences in chronological changes at each time period were found for G-CSF, IL-6, and IL-1β. Furthermore, IL-1β and G-CSF chronologically and similarly changed between model mice and patients with LC after BMC infusion. With respect to the $F(h)_j$ for human G-CSF and human IL-1β (vectors indicating chronological changes), Table 2 shows a decrease for f_1 (two-dimensional x component) and an increase for f_2 (two-dimensional y component). Human serum G-CSF and IL-1β levels decreased from before to 1 day after ABM*i*, but IL-1β increased from 1 day to 1 week after ABM*i*, whereas G-CSF levels did not change. These results indicate that ABM*i* transiently downregulated G-CSF and IL-1β at 1 day after infusion in both patients and model mice and that infused BMCs repair the cirrhotic liver by suppressing the early expression of these cytokines. G-CSF and IL-1β in sera of LC patients without ABM*i* therapy were not changed 1 week after admission (data not shown). However, proving that the BMC infusion caused these cytokine changes in the